

Silica Orthorhombic Mesoporous Films with Low Refractive Index and High Thermal Stability

Paolo Falcaro, David Grosso, Heinz Amenitsch, and Plinio Innocenzi*

Dipartimento di Ingegneria Meccanica, settore materiali, Università di Padova, Via Marzolo 9, 35131 Padova, Italy, Lab. Chimie de la Matière condensée, Université Paris 6, 4 Place Jussieu, 75252 Paris Cedex 05, France, Institute of Biophysics and X-ray Structure Research, Austrian Academy of Sciences, Schmiedelstrasse 6, A-8042 Graz, Austria, and Laboratorio di Scienza dei Materiali e Nanotecnologie, Dipartimento di Architettura e Pianificazione, Università di Sassari, Palazzo Pou Salid, Piazza Duomo 6, 07041 Alghero (Sassari), Italy

Received: December 7, 2003; In Final Form: April 28, 2004

Silica mesoporous films have been synthesized via Evaporation Induced Self-Assembling (EISA) using Pluronic F-127 as a templating agent and mesostructures with *Fmmm* orthorhombic symmetry have been obtained. An optimized thermal process to stabilize the silica walls has been used; the silica films exhibited an excellent thermal stability in a large range of temperatures and the mesostructure remained organized up to 950 °C. Fourier transform infrared spectroscopy has shown that the high thermal stability is correlated with a progressive strengthening of the silica structure during thermally-induced polycondensation reactions and structural rearrangements of 4-fold rings present in the silica walls. The mesostructure after annealing at 850 °C is free of silanols and still maintains a high degree of order. The refractive index, volume porosity, and shrinkage have been studied as a function of the thermal treatment up to 1050 °C. The films have a low refractive index (1.32), upon removal of the organic template via thermal calcination, and show a 30% residual porosity up to 850 °C.

Introduction

Several types of self-assembled mesoporous materials have been synthesized in recent years¹ and interesting perspectives have been opened to fabricate different optical,^{2,3} electronic,⁴ and sensing devices.⁵ Mesoporous films are particularly appealing for their potential applications in microelectronics and photonics, even if they are more difficult to prepare with respect to powders because high control of self-assembling is required. Recent works have clearly outlined the relationships between the synthesis conditions and the final mesophase.⁶ A good control of pore size, orientation, and connectivity has been achieved and lamellar, bidimensional (2D) hexagonal, three-dimensional (3D) hexagonal, or cubic mesophases are commonly obtained. Extensive studies have clarified a great part of the processes that are beneath the evaporation-induced self-assembling (EISA)⁷ of oxide and hybrid organic–inorganic films.

Another critical point is the template removal and stabilization of the mesostructure. This feature is not less important than controlling synthesis and film preparation; practical use of mesoporous films requires a highly stable material whose properties should be well controlled. The organic template can be removed via chemical extraction,⁸ ozone treatment,⁹ photocalcination,¹⁰ and thermal calcination. The choice of the treatment is very much dependent on the type of surfactant employed for self-assembling, that is, ionic or block copolymers, and on the required properties for the final application. After removal of the template the next step is the stabilization of the mesophase. While most of the research has been focused on the mechanisms of EISA very few works have been addressed

to investigate the properties of the frame that is shaping the mesostructure^{11,12,13} with its stability with time and temperature. The inorganic structure is, in fact, built by self-assembly of oligomeric oxohydroxo species on the micelle surface. During the film deposition, evaporation of the solvent induces assembling and condensation of the inorganic species. A larger degree of condensation in the inorganic frame is generally achieved via specific thermal treatments that simultaneously remove the organic template and induce the condensation reactions. The mesophase will be, however, strongly affected, and a strong reduction of the surface area and porosity will be observed. In general, the stabilization of the oxide frame is more difficult to achieve when ionic surfactants have been employed for EISA. This is in large part a consequence of the small wall thickness. An improved thermal stability has been observed upon treatment of powders and films with tetraethyl orthosilicate vapors.^{11,12,13}

Important potential applications for silica mesoporous films are low refractive index materials¹⁴ and ultralow-k dielectrics.¹⁵ Because of the large demand from industry of new and advanced materials with highly-performing functionalities, these films can open the way to new devices with simple architectures that are compatible with the widely-used silica on silicon technologies. It is important, therefore, to fabricate films whose mesostructure is thermally stable, the silica skeleton is fully densified, and are without residual hydroxyl groups on the surface.

In the present work silica mesoporous films with an orthorhombic mesostructure have been synthesized via EISA. The goal has been to reach full control of the mesostructure at the different firing temperatures to obtain the largest thermal stability without losing the order and a low refractive index. Fourier transform infrared spectroscopy, small-angle X-ray diffraction,

* Corresponding author: E-mail, plinio@uniss.it; Fax, +39-079-9720420.

and variable angle spectroscopy ellipsometry have been used in combination to study the evolution of the silica frame, porosity, refractive index, and porous structure with the temperature.

Experimental Procedure

Materials. Pluronic F127 ($\text{OH}(\text{CH}_2-\text{CH}_2\text{O})_{106}(\text{CHCH}_3-\text{CH}_2\text{O})_{70}(\text{CH}_2\text{CH}_2\text{O})_{106}\text{H}$) and tetraethyl orthosilicate (TEOS) were purchased from Aldrich and used as received. Ethanol was obtained from Prolabo. Employed as the substrate were 100 oriented, P-type/Boron doped silicon wafers.

Synthesis. A stock solution was prepared by adding (in the following order) ethanol, TEOS, water, and HCl in the molar ratios $\text{TEOS}:\text{EtOH}:\text{H}_2\text{O}:\text{HCl} = 1:2.78:1.04:56.2 \cdot 10^{-3}$. The sol was left to react under stirring 1 h at room temperature. A second solution was prepared by dissolving 1.3 g of Pluronic F-127 in 15 cm^3 of EtOH and 1.5 cm^3 of acid aqueous solution. Pluronic F-127 block-copolymers ($\text{EO}_{106}-\text{PO}_{70}-\text{EO}_{106}$) were obtained from Aldrich and used as received. The final sol was obtained by adding 7.7 cm^3 of the stock sol to the solution containing the block copolymer. The final solution, with molar ratios $\text{TEOS}:\text{EtOH}:\text{H}_2\text{O}:\text{HCl}:\text{Pluronic F127} = 1:16.3:5.4:56.5 \cdot 10^{-3}:5 \cdot 10^{-3}$, was reacted under stirring 24 h and then was aged at 28°C for one week.

Mesostructured silica films were deposited via dip-coating in controlled conditions of humidity and temperature. All of the depositions were performed at 30% RH, with a withdrawal speed of 20 cm min^{-1} and 28°C . After the deposition the films were maintained in the deposition chamber for 10 min and then fired at 150°C for 1 h in air. Thermal treatments at higher temperatures were performed introducing the samples directly in the oven. The firing process was done in sequence, that is, all of the samples were fired at 150°C , then at 250°C , and so on, up to 1050°C .

Characterizations. The structural evolution in silica films was followed using a Perkin-Elmer 2000 Fourier transform infrared (FTIR) spectrophotometer. The spectra are the average of 128 scans with 2 cm^{-1} of resolution.

The mesostructure in films deposited on silicon substrates was investigated using high-flux grazing incidence small-angle X-ray scattering (GISAXS) apparatus at the Austrian high-flux beamline of the electron storage ring ELETTRA (Trieste, Italy),¹⁶ taking for each image the average of 10 single acquisitions and 3 s of exposition time. The instrumental grazing angle was set up maintaining an incident X-ray beam (wavelength 1.54 \AA) smaller than 3° . From the recording of the CCD detector (1024×1024 pixels, Photonic Science) the *in* and *out of plane* diffraction maxima were observed.

Refractive index and thickness were measured by a variable angle spectroscopy ellipsometry (VASE) (Wollam Instruments). Optical properties were deduced by fitting the obtained ellipsometric ψ and Δ optical quantities, measured at 10 nm intervals, between 400 and 1400 nm, for 53° , 56° , and 59° incidence angles. Residual porosity of the films was calculated from the refractive index data obtained by ellipsometry using the Lorentz–Lorenz formula.

Results and Discussion

FTIR Study of Evolution of Silica Structure with Temperature. FTIR spectroscopy is a simple and effective analytical tool to study the structure of sol–gel processed¹⁷ and self-assembled materials.¹⁸ In the case of thin films, absorption spectra give a direct and fast snapshot of the condensation state of the oxide network. Other techniques, such as solid-state NMR

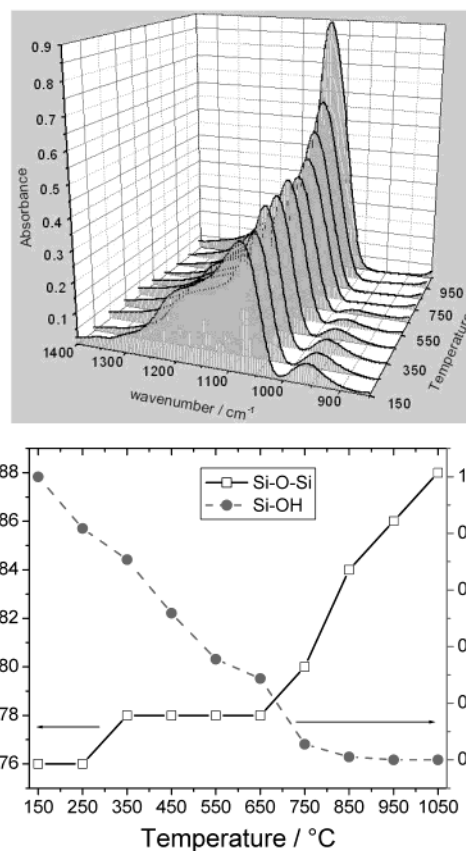


Figure 1. (a) FTIR absorption spectra, in the range, $1400\text{--}850 \text{ cm}^{-1}$, of silica mesostructured films treated at different temperatures. (b) Change of the $\nu_{as}(\text{Si-O-Si})$ wavenumber and Si-OH intensity as a function of the thermal treatment.

or absorption methods cannot be, in fact, applied to thin films or result in little informative.

Figure 1a shows the FTIR absorption spectra in the range $1400 - 850 \text{ cm}^{-1}$ as a function of annealing temperature. The main intense absorption band around 1070 cm^{-1} is attributed to antisymmetric $\nu_{as}(\text{Si-O-Si})$ stretching.¹⁷ This band increases in intensity and shifts to larger wavenumbers at higher temperatures. The intense broad shoulder around 1200 cm^{-1} , accompanying the $\nu_{as}(\text{Si-O-Si})$ stretching mode, is attributed in the literature to a broadened signature of the longitudinal optical (LO) component of the transverse optical (TO) anti-symmetric stretching, or a mixed LO-TO mode with a dominant LO character.¹⁹ The vibrational mode at 950 cm^{-1} is assigned to Si-OH stretching;¹⁷ this band decreases in intensity with the increase of the firing temperatures. The changes as a function of the temperature of the $\nu_{as}(\text{Si-O-Si})$ wavenumber and Si-OH intensity are shown in Figure 1b. The shift of the $\nu_{as}(\text{Si-O-Si})$ mode to larger wavenumbers is a clear indication of the silica structure strengthening with the proceedings of the polycondensation reactions; this is always accompanied by a decrease in the intensity of the Si-OH band (950 cm^{-1}). After 750°C the Si-OH bands disappeared while a steady increase of the $\nu_{as}(\text{Si-O-Si})$ vibration wavenumber to larger values was observed. A full condensation in the silica network is, therefore, reached at temperatures higher than 750°C . At these temperatures, however, the mesostructure is still present and well organized, as shown by SAXS measures (vide infra). Small firing steps allow a progressive reduction of silanol groups up to 850°C (Figure 1) and the silica network forming the walls can evolve during the firing process to a stronger, denser, and more stable structure.

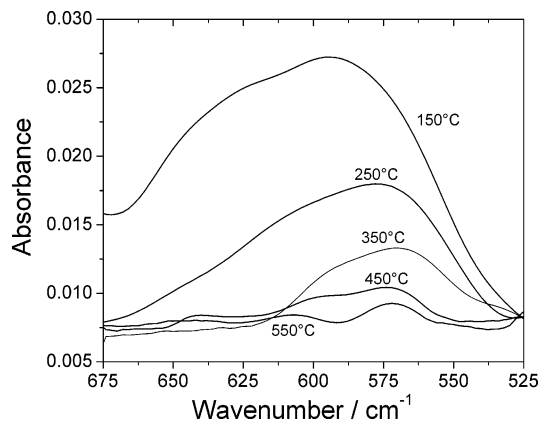


Figure 2. FTIR absorption spectra, in the range, 675–525 cm^{-1} . The change in the absorption intensity of 4-fold silica rings' vibrational modes ($\sim 590 \text{ cm}^{-1}$) as a function of the calcination temperature is shown.

Comparison of FTIR Spectra of Pluronic and CTAB Self-Assembled Films. In a previous work we underlined that FTIR spectra of EISA mesostructured silica films show some distinctive features – the presence of 4-fold rings and disorder-induced vibrational modes.¹⁸ The FTIR spectra of silica mesostructured films synthesized from ionic surfactants, such as cetyltrimethylammoniumbromide (CTAB), show a characteristic fingerprint in the 950–1250 cm^{-1} region (the preparation of these films can be found in Innocenzi et al.¹⁸). These spectra are linked with the structure of the silica walls, because the walls in CTAB films are not very thick ($\sim 2 \text{ nm}$), the structure cannot, in fact, assume any configuration and meets some physical constraints to rearrange. Doshi et al.²⁰ have experimentally supported the hypothesis that basically 4-fold rings are found in the silica walls. The presence of 4-fold rings in the structure is generally revealed by an absorption band around 600 cm^{-1} , while identification of this species through the band in the 1000–1200 cm^{-1} is much more controversial and requires complex deconvolution methods.^{18,21} (A detailed discussion and attribution of the different infrared vibrational modes in CTAB mesostructured films within the 1000–1200 cm^{-1} region can be found in our previous work, Innocenzi et al.¹⁸). The absorption band around 600 cm^{-1} is, therefore, assigned to vibrations of four-member rings within the ring plane – Si–O stretching vibrations coupled with O–Si–O and Si–O–Si bending vibrations.²² Figure 2 shows the evolution of this band with temperature. At 550 $^{\circ}\text{C}$ the vibrational mode due to 4-fold rings is no longer detected. This is an indication that at this temperature 4-fold rings can rearrange into structures where the silica intertetrahedral bonds are less strained. A comparison of FTIR spectra of self-assembled silica CTAB (Figure 3a and Pluronic F-127 (Figure 3b) films show substantial differences. Because of the greater thickness of the walls ($\sim 8 \text{ nm}$), measured by TEM (not shown in the Figures), which is typically four times larger than CTAB films, Pluronic F-127 films spectra exhibit only the $\nu_{as}(\text{Si}-\text{O}-\text{Si})$ mode and the related LO shoulder (Figure 3b). The CTAB silica films spectra (the FTIR spectra in Figure 3a) are taken for comparison from the data of Innocenzi et al.¹⁸) are, instead, much more complicated due to the overlapping of different modes attributed to the simultaneous presence of 4-fold rings and disorder-induced modes.^{18,17} The larger thermal instability of CTAB-derived EISA films is, therefore, due to the small wall thickness.²³ An enhanced thermal stability in silica CTAB EISA films was, in fact, achieved by Tanaka et al.^{11,12,13} via TEOS vapor exposure to increase the pore wall thickness and condense the network to a larger extent.

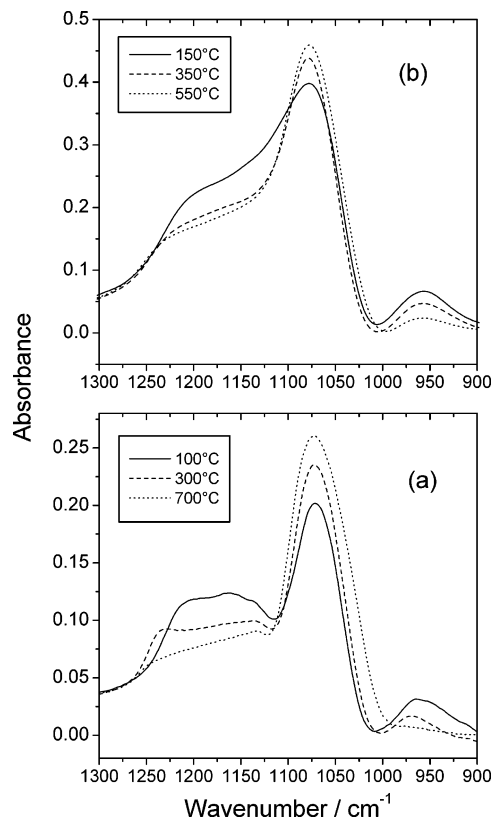


Figure 3. FTIR absorption spectra, in the 1300–900 cm^{-1} region, of mesoporous silica films prepared using Pluronic F-127 (a) and CTAB (b) as templating agents. Data in Figure 3(a) are taken from Innocenzi et al.¹⁸

Synthesis of self-assembled silica films from Pluronic F-127 has, therefore, the general advantage that other treatments to increase the thermal stability are not potentially necessary.

Thermal Dehydroxylation. Figure 4a shows the FTIR absorption spectra of silica mesostructured films in the range 3850–2650 cm^{-1} . Two overlapped regions of vibrational modes can clearly be distinguished. The first one in the lower wavenumber range (within the dot rectangle in Figure 4a), is due to absorption of organic groups in Pluronic F127, can be taken as a signature of the presence of the block copolymer within the material, and a second one at higher wavenumbers is due to hydroxyl absorptions. This second broad band is composed of several overlapped bands assigned to different types of hydroxyl vibrations.²⁴ In particular, three overlapped vibrational modes at 3743, 3676, and 3635 cm^{-1} are observed at the low wavenumber side (Figure 4b). The bands, on the basis of the literature,²⁵ are assigned as follows: 3743 cm^{-1} , free single silanol groups; 3676 cm^{-1} , pairs of silanols mutually hydrogen-bonded in linear configuration, where only one is participating in the hydrogen bonding (oxygen atoms form H-bonds with a hydrogen atom of an adjacent silanol); 3635 cm^{-1} , pairs of silanols mutually hydrogen-bonded in a linear configuration, where only one is participating in the hydrogen bonding (hydrogen atoms form H-bonds with an oxygen atom of an adjacent silanol). These bands appear only after thermal treatments above 150 $^{\circ}\text{C}$; at this temperature these absorption bands are not observed, in fact, in the films. The three bands also increased in intensity from 250 to 450 $^{\circ}\text{C}$, and then they reversed the trend. The block-copolymer is progressively eliminated with the increase of the temperature of calcination, but weak traces of Pluronic F-127 are still observed even after annealing at 550 $^{\circ}\text{C}$ (Figure 1). These results are in good

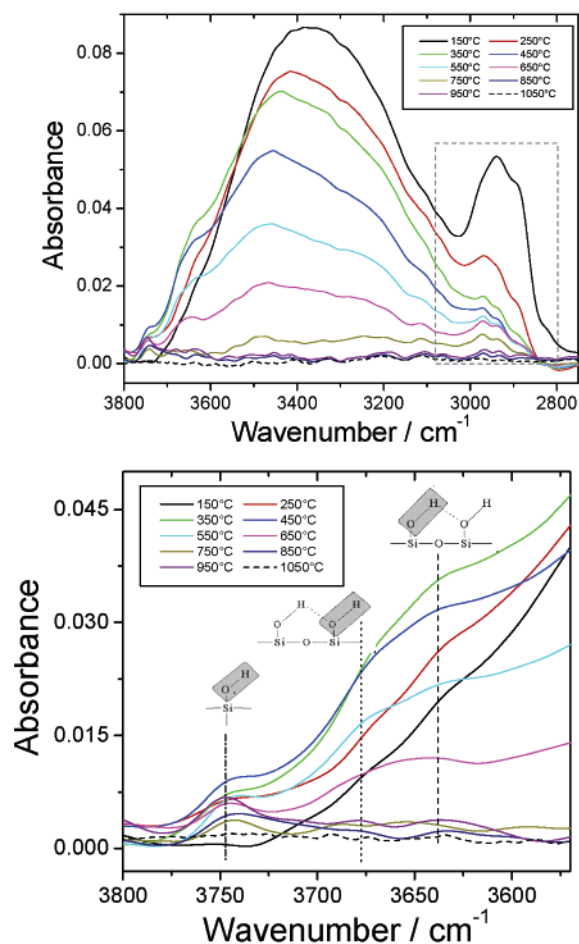


Figure 4. (a) Thermal dehydroxylation process observed by FTIR absorption spectra, as a function of the calcination temperature. (b) Details of the overlapped absorption modes in the 3800–3570 cm^{-1} region.

agreement with the finding of Kleitz et al.²⁶ during calcination of SBA materials templated with triblock copolymers. The absorption maximum of the broad band peaking around 3370 cm^{-1} is progressively shifted to higher wavenumbers and decreases in intensity at larger temperatures of annealing. This band is due to hydrogen-bonded silanols in chains that contain more than a pair of mutually H-bonded OH groups and the shift is an indication of the progressive condensation of the silanol species with a decrease in the length of the silanol chains.

It is interesting to note that while the thermal dehydroxylation of the silanol species present in hydrogen-bonded chains or silanol pairs is completed at 750 °C, to eliminate the single silanols formed during dehydroxylation larger temperatures are required. In the range of temperatures 750–950 °C only isolated silanols are detected because residual isolated silanols are more difficult to remove due to the lower possibility to condense.

Film Mesostructure and Its Evolution with Annealing.

The study of the mesophase in the films was done by grazing incidence and transmission SAXS using synchrotron radiation. The diffraction patterns of silica films on thin silicon substrates (20 μm thickness) allowed us to obtain the Bragg and Laue reflections; a “distorted $Im\bar{3}m$ ” mesophase symmetry was detected. The formation of distorted cubic mesostructures was already described in mesostructured films^{27,28} and is due to the uniaxial contraction of the films in a direction normal to the substrate. This contraction is generally reflected in a high loss of symmetry; some authors have described the distorted $Im\bar{3}m$ structure as triclinic, without however a specific identification

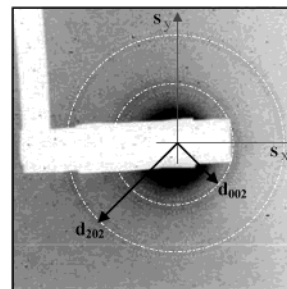


Figure 5. SAXS transmission diffraction pattern of an F-127 silica mesostructured film upon drying at 60 °C. A cubic $Im\bar{3}m$ symmetry is observed.

of the structure.²⁷ The thermal treatment employed induces the symmetry change from cubic up to orthorhombic order, while this kind of deformation is only weakly appreciable for lower thermal treatments (up to 150 °C), the contraction is continuous during all the thermal treatment.

The identification of the mesophase as a cubic one is confirmed by the transmission SAXS image (60 °C sample) where the interplanar distance d_{200} and d_{202} are representative of a cubic cell: $d_{002}:d_{202} = 1:\sqrt{3}$ (Figure 5) (Remark: The indexing was performed on the ground of the equivalent orthorhombic unit cell). In a phase transition from a body-centered cubic cell ($Im\bar{3}m$ in the space group) only a few new symmetries are allowed by group theory and if we consider all the transitions, the possible crystal lattices that we should find are the $Fm\bar{3}m$ and $Fddd$ (in the space group), which are both orthorhombic. From a computer simulation, done using the CMPR program (B.Toby, NIST), only the $Fm\bar{3}m$ diffraction patterns fit the recorded spot positions. The simulation was performed using $a = 21$ nm, $b = 18$ nm, and $c = 29.7$ nm ($=\sqrt{2}a$), as cell parameters; at the end of the simulation a list of the allowed hkl Miller indices and the corresponding coordinates (d -space and angle) are obtained. These reflection coordinates have been transferred to cylindrical coordinates which are observed in the surface diffraction experiment ($s_r = \sqrt{s_x^2 + s_y^2}$, s_z) and visualized in an image (Figure 6a). Comparing the simulated image with the diffraction spots from the SAXS experiments (Figure 6b), a very good correspondence is achieved by iterating the lattice parameters a , b , and c to the final values quoted above. This attribution is also in good agreement with the electron diffraction experiments of Besson et al.²⁹ with Pluronic F68 silica orthorhombic films. Cubic mesostructures are preferred because of the highest symmetry and thermal stability; in general, if the same amphiphilic block copolymer is used to template hexagonal or cubic structures, the cubic mesostructures show the highest thermal stability because of the larger pore walls.

On the basis of the allowed transition, from $Im\bar{3}m$ to $Fm\bar{3}m$, the mesophase evolution has been represented in Figure 7; the new cell parameters with their orientation with respect to the substrate are shown. The phase change is due to a distortion of the structure during the thermal shrinkage and is therefore a process that happens as a smooth transition with the increase of the calcination temperature. The scheme in Figure 7 shows only the initial and final cells of the phases. This hypothesis is well supported by the SAXS images taken from the samples after calcination at different temperatures. The evolution of SAXS images of the films during the different firing steps from 150 up to 1050 °C are shown in Figure 8. The SAXS image intensity has been normalized, the spatial distortion has been

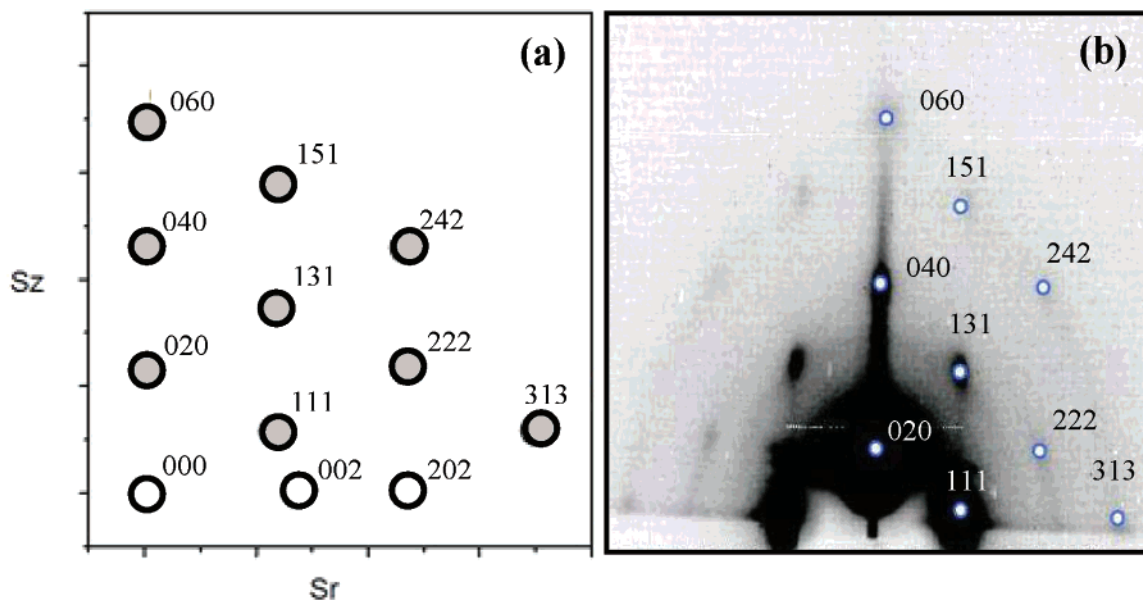


Figure 6. Comparison of a computer-simulated image utilizing the CMPR program, of an *Fmmm* structure with $a = 21$ nm, $b = 18$ nm, and $c = 29.7$ nm as cell parameters (a), with the GISAXS image of a film calcined at 250 °C (b). Indicated are the corresponding s -scales for the cylindrical coordinate system.

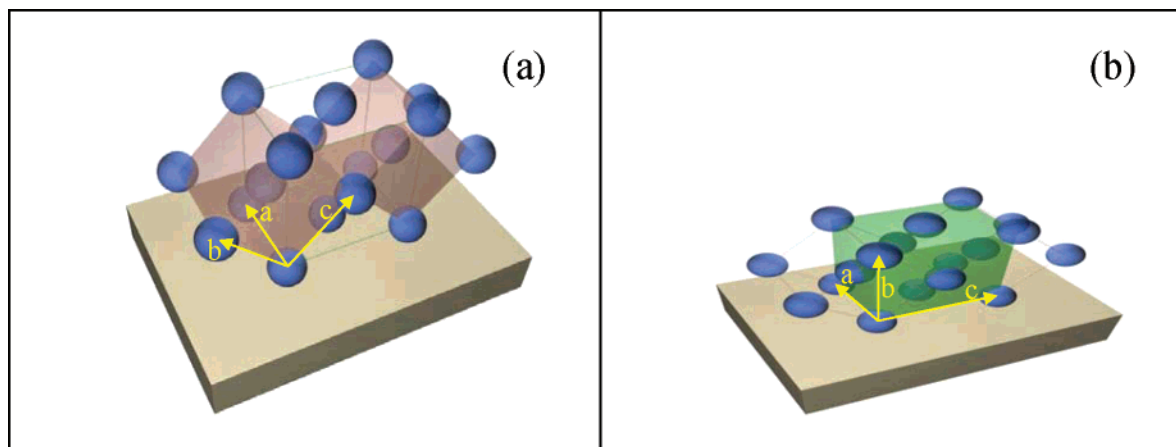


Figure 7. Illustration of the symmetry changes from *Im3m* (a) to *Fmmm* (b).

corrected, and the background has been subtracted. The intensity cannot be, however, quantitatively compared because different instrumental amplifications have been used to avoid the signal saturation in some samples. The patterns appear as a semiellipse with some intense spots attributed to diffraction maxima: 002, 111, and 020 distances of planes in the mesostructure (see Figure 6). These spots allow quantifying of the contraction due to the thermal effect. The position change of the 020 spot indicates a change of the b parameter; the trend is appreciable from Figure 8 where the distance from the beam center increase for each thermal step. For each CCD image shown in Figure 8, using the FIT2D program (A. P. Hammersley/ESRF), a radial integration has been done. To find the right peak position of the 020 spot, all the other spots have been masked. This procedure allowed the determination of the d spacing plotted in Figure 9 and the lattice parameter b (Figure 10). In the SAXS patterns at 150, 250, and 350 °C, a larger degree of order is observed, because up to the third-order diffraction maxima are observed. From 550 °C only the first maxima are, instead, detected, with a qualitative increase in the intensity of the ring, which is due to a presence of polyoriented domains. At 1050 °C the mesostructure is collapsed and the 3D order is lost.

The interplanar distances, d_{020} , from which the b parameter is calculated, do not significantly change up to 150 °C. At 350 °C, when the great part of the inorganic template is decomposed, d_{020} shows a sudden decrease, 23% less with respect to 250 °C. This variation continues with an almost linear trend up to 850 °C (Figure 9). The other parameters, a and c , do not change with the thermal treatment, in agreement with the orthorhombic cell model where only the parameters with at least one component normal to the substrate must change. At 850 °C the interplanar distance, d_{020} , will change with respect to as deposited film of around 50%.

The SAXS images show some reflection spots, indicated by the 020 $_r$ index, which are observed in the films calcined at lower temperatures.

The change in d_{020} space, measured by SAXS, and the film thickness, measured by ellipsometry, as a function of the annealing temperature are shown in Figure 10. They exhibit a similar trend, with a decrease in thickness and d_{020} space with the temperature. At 1050 °C an abrupt decrease in thickness and of d , with the collapse of the orthorhombic mesostructure, is observed. For the first time a mesostructure with a good order degree is maintained up to 950 °C; all three spots attributed to

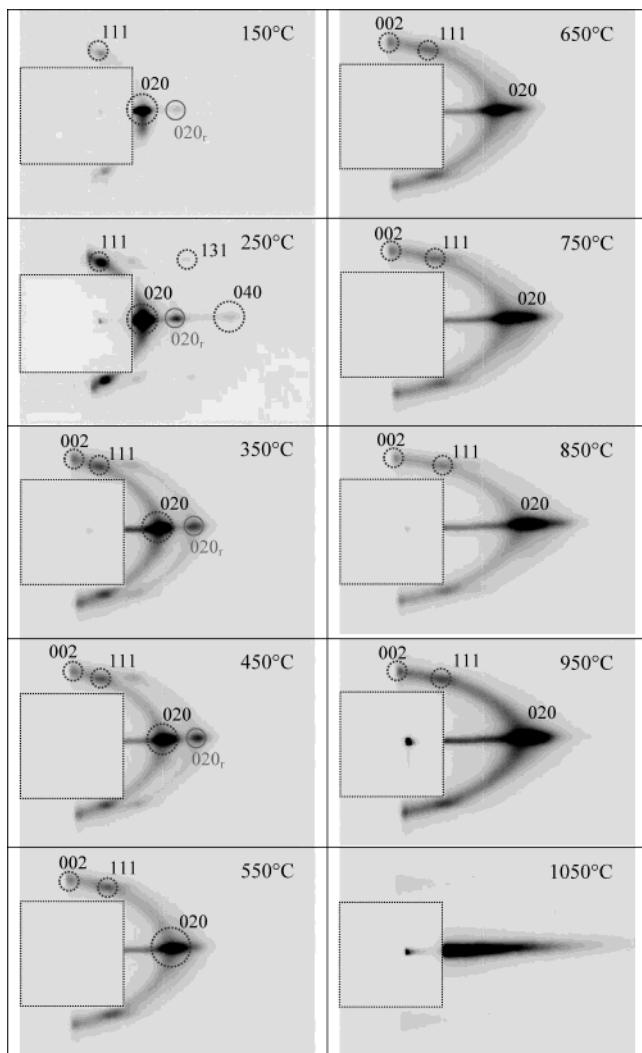


Figure 8. GISAXS images of the films calcined at different temperatures.

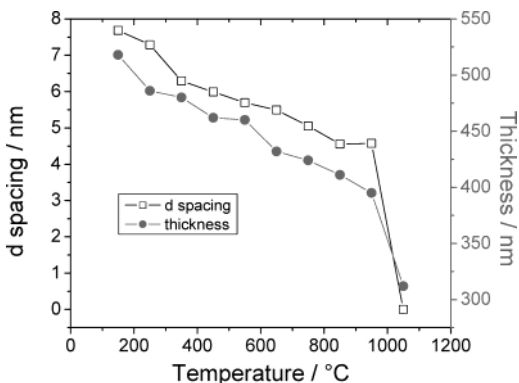


Figure 9. Change of the interplanar distance, d_{020} , and film thickness as a function of the calcination temperature.

d_{002} , d_{111} , and d_{020} are still very distinguishable. The increasing of the ring intensity suggests that an order changing should be imminent. After the last thermal step, for temperatures included between 950 °C and 1050 °C the order was lost (the diffraction spots disappear). An abrupt decrease of thickness and d , the collapse of the mesostructure, is observed. With respect to the parameters measured in as-prepared films, the contraction in the direction normal to the substrate was around 50% in agreement with the literature.

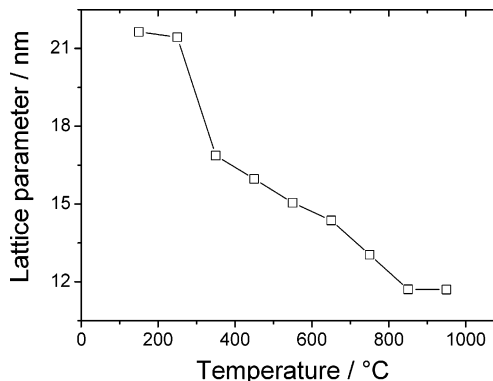


Figure 10. Change of the lattice parameter, b , as a function of the calcination temperature.

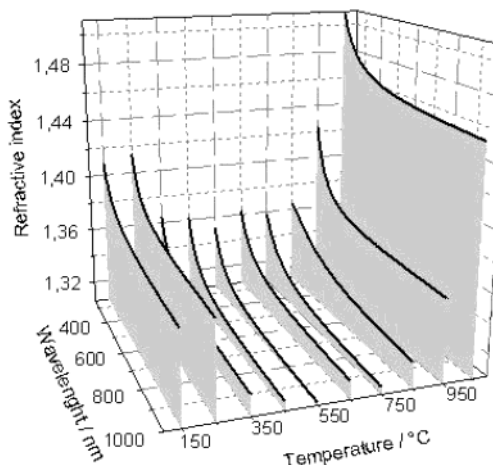


Figure 11. Dispersion of the refractive index in the films after thermal calcination at different temperatures.

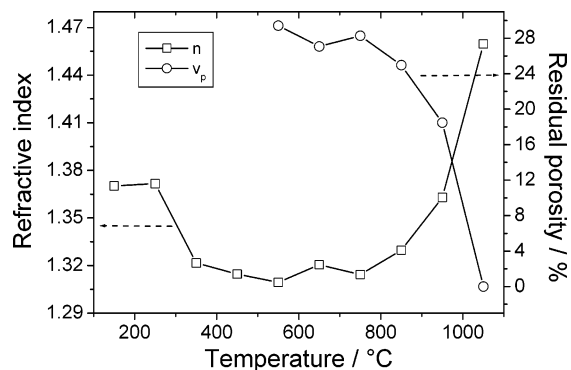


Figure 12. Volume fraction of residual pores, V_p , and refractive index, n , at 633 nm as a function of the calcination temperature.

Refractive Index and Residual Porosity. The dispersion of the refractive index from 200 to 1000 nm as a function of the annealing temperature is shown in Figure 11. The detailed trend of the change in refractive index with a temperature at a selected wavelength ($\lambda = 633$ nm) is shown in Figure 12. A decrease in refractive index from 1.37 to 1.32 is observed after full removal of the organic template. After this decrease the value remained constant in the range 350 – 750 °C, to increase again from 850 °C because of the pore shrinkage and collapse. The value of the refractive index achieved after a calcination at a temperature between 350 and 750 °C is low enough to consider these mesostructured silica films as low-refractive-index materials that can be suitable for several optical applications. At 1050 °C the refractive index was 1.46 corresponding to the value of

the dense silica; this is an indication of pore collapse and complete densification of the films, without any cracking. In the same Figure the change in porosity of the samples fired from 650 up to 1050 °C is also shown. The volume fraction of the residual pores, V_p , was calculated from the refractive index at 633 nm, measured by ellipsometry, using the Lorentz–Lorenz equation³⁰

$$(n_f^2 - 1)/(n_f^2 + 2) = (1 - V_p)(n_{\text{SiO}_2}^2 - 1)/(n_{\text{SiO}_2}^2 + 2) \quad (1)$$

with n_f the measured refractive index of the film and taking $n_{\text{SiO}_2} = 1.459$ as the refractive index of the fully densified silica. The porosity of the films in which the organic template was not yet completely removed was not calculated. At 650 °C the porosity is around 30%, at 950 °C it is reduced to 15%, and with the mesostructure collapse the films are fully densified. It is interesting to observe that the empirical relationship between refractive index, n , and the porosity volume fraction, V_p ,

$$n = 1.458 - 0.458V_p \quad (2)$$

that has been found for silica xerogel materials is still valid for mesostructured porous silica films (with an error of ± 0.01).

Conclusions

Silica mesostructured films with a highly-organized orthorhombic structure have been prepared via EISA dip-coating. An optimized thermal treatment applied to the silica mesostructured films enhanced the thermal stability of the organized phase up to 950 °C. A progressive thermal treatment, with different increasing steps of 100 °C, allowed controlling the condensation and the thermal dehydroxylation of the silica walls. The stabilized orthorhombic phase shows a refractive index as low as 1.32 in a wide range of temperatures.

Acknowledgment. Italian MIUR through FIRB (RBNE01P4JF) projects is acknowledged for financial support.

References and Notes

- (1) Soler-Illia, G. J. A. A.; Sanchez, C.; Lebeau, B.; Patarin, J. *Chem. Rev.* **2002**, *102*, 4093.
- (2) Brian, S. J.; Wirnsberger, G.; McGehee, M. D.; Chmelka, B. F.; Stucky, G. D. *Adv. Mater.* **2001**, *13*, 1231.
- (3) Scott, B. J.; Wirnsberger, G.; Stucky, G. D. *Chem. Mater.* **2001**, *13*, 3140.
- (4) Fan, H. Y., *J. Non-Cryst. Solids* **2001**, *285*, 79.
- (5) (a) Innocenzi, P.; Martucci, A.; Guglielmi, M.; Bearzotti, A.; Traversa, E. *Sens. Actuators, B* **2001**, *76*, 299. (b) Bearzotti, A.; Mio Bertolo, J.; Innocenzi, P.; Falcaro, P.; Traversa, E. *J. Eur. Ceram. Soc.* **2003**, *24*, 1969. (c) Bearzotti, A.; Mio Bertolo, J.; Innocenzi, P.; Falcaro, P.; Traversa, E. *Sens. Actuators, B* **2003**, *95*, 107.
- (6) (a) Grosso, D.; Babonneau, F.; Sanchez, C.; Soler-Illia, G. J. A. A.; Crepaldi, E. L.; Albouy, P. A.; Amenitsch, H.; Balkenende, A. R.; Brunet-Bruneau, A. *J. Sol-Gel Sci. Technol.* **2003**, *26*, 561. (b) Besson, S.; Gacoin, T.; Ricolleau, C.; Jacquod, C.; Boilot, J. P. *J. Mater. Chem.* **2003**, *13*, 404. (c) Cagnol, F.; Grosso, D.; Soler-Illia, G. J. A. A.; Crepaldi, E. L.; Babonneau, F.; Amenitsch, H.; Sanchez, C. *J. Mater. Chem.* **2003**, *13*, 61. (d) Gibaud, A.; Grosso, D.; Smarsly, B.; Baptiste, A.; Bardeu, J. F.; Babonneau, F.; Doshi, D. A.; Chen, Z.; Brinker, C. J.; Sanchez, C. *J. Phys. Chem. B* **2003**, *107*, 6114. (e) Doshi, D. A.; Gibaud, A.; Liu, N.; Sturmayer, D.; Malanoski, A. P.; Dunphy, D. R.; Chen, H.; Narayan, S.; MacPhee, A.; Wang, J.; Reed, S. T.; Hurd, A. J.; Van Swol, F.; Brinker, C. J. *J. Phys. Chem. B* **2003**, *107*, 7683.
- (7) Brinker, C. J.; Lu, Y.; Sellinger, A.; Fan, H. *Adv. Mater.* **1999**, *11*, 579.
- (8) Grosso, D.; Balkenende, A. R.; Albouy, P. A.; Ayrat, A.; Amenitsch, H.; Babonneau, F. *Chem. Mater.* **2001**, *13*, 1848.
- (9) Clark, T.; Ruiz, J. D.; Fan, H.; Brinker, C. J.; Swanson, B. I.; Parikh, A. N. *Chem. Mater.* **2000**, *12*, 3879.
- (10) (a) Hozumi, A.; Yokogawa, Y.; Kameyama, T.; Hiraku, K.; Sugimura, H.; Takai, O.; Okido, M. *Adv. Mater.* **2000**, *12*, 985. (b) Gomez Vega, J. M.; Iyoshi, M.; Kim, K. Y.; Hozumi, A.; Sugimura, H.; Takai, O. *Thin Solid Films* **2001**, *398*, 615.
- (11) Ryoo, R.; Ko, C. H.; Kim, J. M. *J. Phys. Chem. B* **1997**, *101*, 10610.
- (12) Nishiyama, N.; Tanaka, S.; Egashira, Y.; Oku, Y.; Ueyama, K. *Chem. Mater.* **2002**, *14*, 4229.
- (13) Tanaka, S.; Nishiyama, N.; Oku, Y.; Egashira, Y.; Ueyama, K. *Microp. Mesop. Mater.* **2003**, *63*, 105.
- (14) Zhang, Q.; Wang, J.; Wu, G.; Shen, J.; Buddhudu, S. *Mater. Chem. Phys.* **2001**, *72*, 56.
- (15) Jain, A.; Rogojevic, S.; Ponoht, S.; Agarwal, N.; Matthew, I.; Gill, W. N.; Persans, P.; Tomozawa, M.; Plawsky, J. L.; Simonyi E. *Thin Solid Films* **2001**, *398*, 513.
- (16) Amenitsch, H.; Rappolt, M.; Kriechbaum, M.; Mio, H.; Laggner, P.; Bernstorff, S. *J. Synchrotron Radiation* **1998**, *5*, 506.
- (17) Innocenzi, P. *J. Non-Cryst. Solids* **2003**, *316*, 309.
- (18) Innocenzi, P.; Falcaro, P.; Grosso, D.; Babonneau, F. *J. Phys. Chem. B* **2003**, *107*, 4711.
- (19) Almeida, R. M.; Pantano, C. G. *J. Appl. Phys.* **1990**, *68*, 4225.
- (20) Doshi, D. A.; Gibaud, A.; Goletto, V.; Lu, M.; Gerung, H.; Ocko, B.; Han, S. M.; Brinker, C. J. *J. Am. Chem. Soc.* **2003**, *125*, 11646.
- (21) Fidalgo, A.; Ilharco, L. M. *J. Non-Cryst. Solids* **2003**, *316*, 309.
- (22) Yoshino, H.; Kamiya, K.; Nasu, H. *J. Non-Cryst. Solids* **1990**, *126*, 68.
- (23) Davidson, A. *Curr. Opin. Coll. Interface Sci.* **2000**, *7*, 92.
- (24) (a) Chen, J.; Li, Q.; Xu, R.; Xiao, F. *Angew. Chem.* **1995**, *34*, 2694. (b) Plotnichenko, V. G.; Sokolov, V. O.; Dianov, E. M. *J. Non-Cryst. Solids* **2000**, *261*, 186. (c) Davis, K. M.; Tomozawa, M. *J. Non-Cryst. Solids* **1996**, *201*, 177.
- (25) (a) Zhao, X. S.; Lu, G. Q.; Whittaker, A. K.; Millar, G. J.; Zhu, H. Y. *J. Phys. Chem. B* **1997**, *101*, 6525. (b) Chen, J.; Li, Q.; Ding, H.; Pang, W.; Xu, R. *Langmuir* **1997**, *13*, 2050. (c) Jentus, A.; Kleestorfer, K.; Vinek, H. *Microp. Mesop. Mater.* **1999**, *27*, 321.
- (26) Kleitz, F.; Schmidt, W.; Schuth F. *Microp. Mesop. Mater.* **2003**, *65*, 1.
- (27) Crepaldi, E. L.; Soler-Illia, G. J. A. A.; Grosso, D.; Cagnol, F.; Ribot, F.; Sanchez, C. *J. Am. Chem. Soc.* **2003**, *125*, 9770.
- (28) Crepaldi, E. L.; Soler-Illia, G. J. A. A.; Grosso, D.; Durand, D.; Sanchez, C. *Angew. Chem., Int. Ed.* **2003**, *42*, 347.
- (29) Besson, S.; Ricolleau, C.; Gacoin, T.; Jacquod, C.; Boilot, J.-P. *Microp. Mesop. Mater.* **2003**, *60*, 43.
- (30) Born, M.; Wolf, E. in *Principles of Optics*; Pergamon Press: New York 1975; p.87.